

# Arc Statistics in Clusters: Galaxy Contribution

Ricardo A. Flores

Department of Physics and Astronomy, University of Missouri–St.Louis

St.Louis, MO 63121-4499

Electronic mail: Ricardo.Flores@umsl.edu

Ariyeh H. Maller

Physics Department, University of California–Santa Cruz

Santa Cruz, CA 95064

Electronic mail: maller@physics.ucsc.edu

and

Joel R. Primack

Physics Department, University of California–Santa Cruz

Santa Cruz, CA 95064

Electronic mail: joel@ucolick.org

Received \_\_\_\_\_; accepted \_\_\_\_\_

## ABSTRACT

The frequency with which background galaxies appear as long arcs as a result of gravitational lensing by foreground clusters of galaxies has recently been found to be a very sensitive probe of cosmological models by Bartelmann et al. (1998). They have found that such arcs would be expected far less frequently than observed (by an order of magnitude) in the currently favored model for the universe, with a large cosmological constant  $\Omega_\Lambda \sim 0.7$ . Here we analyze whether including the effect of cluster galaxies on the likelihood of clusters to generate long-arc images of background galaxies can change the statistics. Taking into account a variety of constraints on the properties of cluster galaxies, we find that there are not enough sufficiently massive galaxies in a cluster for them to significantly enhance the cross section of clusters to generate long arcs. We find that cluster galaxies typically enhance the cross section by only  $\lesssim 15\%$ .

*Subject headings:* cosmology: theory—dark matter—gravitational lensing—  
galaxies: clusters: general

## 1. Introduction

The discovery of long arcs in clusters of galaxies (Lynds & Petrosian 1986; Soucail et al. 1987) offered the prospect of using their observed frequency as a tool to test cosmological models, using the paradigm of the frequency of quasar lensing studies set forth by Turner, Ostriker, & Gott (1984). Wu & Mao (1996) were the first to carry out such a study, in order to gauge the influence of a cosmological constant on the observed frequency of arcs in a homogeneous sample of EMSS clusters (Le Fèvre et al. 1994, Lupino et al. 1999). The main conclusion of Wu & Mao (1996) was that in a spatially flat, low-density universe ( $\Omega_m = 0.3$ ) one would observe about twice as many arcs as in an Einstein-de Sitter universe, but still only about a half the observed number of arcs. The discrepancy with the observed number was somewhat larger though: observational restrictions reduce the number considerably (Hattori, Watanabe, & Yamashita 1997), but source evolution increases the number (Hamana & Futamase 1997). A more recent study by Cooray (1999) found the number to be in agreement with observations for a low-density universe (open or flat), if a minimum cluster velocity dispersion of  $\sim 1080$  km/s is assumed. At least 5 of the eight clusters with confirmed arcs, though, have dispersions below this (see Lupino et al. 1999; and references therein). In these studies a given cosmological model enters mostly via the geometry of space-time.

A recent study by Bartelmann et al. (1998), however, finds the predicted number of arcs to be rather sensitive to the differences in the properties of the clusters predicted in different cosmological models. This study has sharpened the conflict between predictions and observations of long arcs for the low-density flat CDM model. They find that an  $\Omega_m = 0.3$  open cold dark matter (OCDM) model produces about as many arcs as are observed, but a spatially flat  $\Omega_m = 0.3$  CDM model ( $\Lambda$ CDM) produces an order of magnitude fewer, and a standard CDM (SCDM) model two orders of magnitude fewer. Unlike previous studies, the

difference in formation epoch and concentration between clusters in different cosmological models was consistently taken into account, and found to be mainly responsible for the drastic differences in their predicted numbers of long arcs. With many independent pieces of evidence indicating that  $\Lambda$ CDM is the only concordant cosmological model (e.g., Bahcall et al. 1999), it is rather surprising that such a model fails so drastically the arc number test. Clearly, a close examination of possible sources of uncertainty is warranted.

One possible source of enhancement in the observed number of arcs is the contribution of the cluster galaxies to the creation of giant arcs. Previous studies (Wu & Mao 1996; Hattori et al. 1997; Hamana & Futamase 1997; Cooray 1999) have treated clusters as smooth mass distributions. The clusters in the dissipationless N-body simulations studied by Bartelmann et al. (1998) have significant substructure, but they could not resolve galaxies. It is therefore desirable to study the magnitude of the effect galaxies would have on the arc abundance in clusters. Including galaxies in cluster lensing studies is not new (see e.g. Grossman & Narayan 1988). Their effect in deep, high-resolution studies of individual clusters, e.g. in A2218 (Kneib et al. 1996), AC114 (Natarajan et al. 1998) and A370 (Bézecourt et al. 1999), has been found to be significant indeed. Here we quantify their effect on arc statistics by calculating the ratio,  $1 + \Delta$ , of the cross section to produce long arcs<sup>1</sup> when cluster galaxies are included to the cross section when they are not. Of course, the comparison is to be made while keeping the projected mass in the field of view fixed. We find that the results for  $\Delta$  are surprisingly small, typically less than 15% (i.e.  $\Delta \lesssim 0.15$ ), although there is considerable scatter. The scatter can easily be reduced by averaging over 10 or so clusters.

We describe the gravitational lensing model we have used to calculate the arc cross

---

<sup>1</sup> We concentrate only on arcs with length-to-width ratio  $\geq 10$  and length  $\geq 8''$ , the criteria of the search in X-ray clusters (Lupino et al. 1999).

section in section 2. We then explore the observational constraints on the various parameters of the model in section 3. Finally, we presents our results in section 4 and conclude with a discussion of our results and the conclusions we draw from them in section 5, where we also comment on the recent work of Meneghetti et al. (1999) on the same problem. We use throughout a Hubble constant  $H_o = 100h$  km/s/Mpc.

## 2. Gravitational Lensing Model

We model the main cluster mass distribution (dark matter plus the hot intracluster gas) using the standard Pseudo Isothermal Elliptical Mass Distribution (PIEMD), for which the bending angle components at position  $(x, y)$  relative to the cluster center are given by (Kassiola & Kovner 1993; Keeton & Kochanek 1998)

$$\theta_x = \frac{b}{(1 - q^2)^{1/2}} \tan^{-1} \left[ \frac{(1 - q^2)^{1/2} x}{\psi + r_{core}} \right], \quad (1)$$

$$\theta_y = \frac{b}{(1 - q^2)^{1/2}} \tanh^{-1} \left[ \frac{(1 - q^2)^{1/2} y}{\psi + q^2 r_{core}} \right], \quad (2)$$

where  $b = 4\pi(\sigma_{cl}/c)^2(D_{LS}/D_{OS})(e/\sin^{-1} e)$  and  $\psi^2 = q^2(x^2 + r_{core}^2) + y^2$ . The cluster has line-of-sight velocity dispersion  $\sigma_{cl}$  and core radius  $r_{core}$ . Its mass distribution has intrinsic and projected axial ratios  $q_3$  and  $q$  respectively, and  $e = (1 - q_3^2)^{1/2}$ .  $D_{OS}$  and  $D_{LS}$  are angular-diameter distances, from the observer to the source and from the lens to the source respectively.

We model galaxies as truncated isothermal spheres (see Kneib et al. 1996), so that the contribution to the bending angle at  $(x, y)$  of a galaxy at  $(x_g, y_g)$  is given by

$$\theta_x^g = b_g \left( \frac{r_{cut}}{r_{cut} - r_{core}^g} \right) \left( \frac{x_g - x}{d} \right) \left[ \frac{(d^2 + r_{core}^{g\ 2})^{1/2} - r_{core}^g}{d} - \frac{(d^2 + r_{cut}^2)^{1/2} - r_{cut}}{d} \right], \quad (3)$$

$$\theta_y^g = b_g \left( \frac{r_{cut}}{r_{cut} - r_{core}^g} \right) \left( \frac{y_g - y}{d} \right) \left[ \frac{(d^2 + r_{core}^{g\ 2})^{1/2} - r_{core}^g}{d} - \frac{(d^2 + r_{cut}^2)^{1/2} - r_{cut}}{d} \right], \quad (4)$$

where  $b_g = 4\pi(\sigma_g/c)^2(D_{LS}/D_{OS})$  and  $d^2 = (x_g - x)^2 + (y_g - y)^2$ . The galaxy has line-of-sight velocity dispersion  $\sigma_g$ , core radius  $r_{core}^g$ , and truncation radius  $r_{cut}$ .

Figure 1 shows results for a fiducial cluster. The values of the various parameters of the model are explained and justified in section 3, and summarized in Table 1. The cluster is at redshift  $z_{cl} = 0.2$ , seen edge-on with  $q = 0.75$ , and has  $\sigma_{cl} = 1200$  km/s and  $r_{core} = 1h^{-1}$  kpc. An Einstein-de Sitter universe and the filled-beam approximation are assumed in the calculation of angular diameter distances. The background cosmological model is not of great importance, since we are here interested in the *difference* in the lensing cross section of clusters to produce long arcs due to the inclusion of galaxies in the clusters.

The top-left panel shows results for a smooth cluster (no galaxies). The shaded area is the region behind which a circular source at redshift  $z_S = 1$ , and of angular radius  $0.5''$ , would be imaged into a long arc farther out in the cluster. The inner (outer) dashed line is the tangential (radial) caustic. The top-right panel shows the same results when the galaxies are taken into account. The total mass inside a  $150'' \times 150''$  field of view centered on the cluster, shown in the bottom panels, has been kept fixed. It can be seen that there is a significant distortion of the tangential caustic, which results in an increased area where the source can be imaged into a long arc. This is shown for the source marked as a filled star (at  $x = 13''$  and  $y = 2''$ ), whose image can be seen in the bottom right panel. Note there that the counter arc, marked by the arrow, would not be seen given the typical magnitude of a long arc. Also, most arcs that appear only when galaxies are taken into account are not formed on top of galaxies, as noted early on by Grossman & Narayan (1988). The circles mark the positions of the galaxies and have radii chosen to roughly correspond to the size of the galaxies in a deep image.

The caustics labeled 1-4 in the top right panel are due to the correspondingly labeled galaxies in the bottom right panel. The bottom left panel shows the critical curves

corresponding to the caustics in the top left (top right) panel as dashed (solid) lines. The outer (tangential) dashed critical curve of the smooth cluster is repeated in the bottom right panel. In general, the galaxies that most distort and enlarge the shaded region in the top left panel are galaxies close to this critical curve.

### 3. Model Parameters

In order to study the properties of images created by the cluster lens model we need to specify all the parameters needed. Here we explain our choices based on what is known about clusters and cluster galaxies.

The sample of clusters searched for long arcs is selected by X-ray flux (strictly speaking, by central surface brightness; see the discussion in Lupino et al. 1999). This is expected to select very massive clusters given the known correlation of X-ray luminosity with  $\sigma_{cl}$  ( $L_x \sim \sigma_{cl}^4$ ) first established by Solinger & Tucker (1972). None of the EMSS clusters with  $L_x < 4 \times 10^{44}$  erg/s show any arcs (Lupino et al. 1999), corresponding to a minimum dispersion  $\sigma_{cl} = 784_{-62}^{+68}$  km/s using the recent analysis of Wu, Xue, & Fang (1999). Indeed, the lowest velocity dispersion of the clusters with arcs is  $\sigma_{cl} \sim 800$  km/s (see Lupino et al. 1999; and references therein). Therefore we consider here clusters with  $\sigma_{cl} \geq 800$  km/s.

The shape of clusters is not known observationally. Lens models that use the projected axial ratio  $q_{BCG}$  of their brightest cluster galaxy (BCG) reproduce rather well the orientation of arcs and arclets in deep, high-resolution studies of clusters (e.g. Kneib et al. 1996, Natarajan et al. 1998). Bézecourt et al. (1999) find a somewhat rounder mass distribution to give a better fit. To the extent that  $q_{BCG}$  is a good guide to  $q$ , the study of Porter, Schneider, & Hoessel (1991) implies  $q \gtrsim 0.6$ . Numerical simulations of clusters find triaxial shapes for galaxy clusters (Thomas et al. 1999), with mean minor/major axial ratio of 0.5

for a low-density universe. It is easy to translate their distribution into the distribution for  $q$  assuming nearly oblate or prolate halos (see Binney 1978), from which we estimate that  $q \sim 0.5 - 0.9$  for most halos, with a median  $q \sim 0.7$ . We use  $q = 0.5, 0.75$  and  $0.9$  as representative values. This range covers the values used in the studies of A370, A2218 and AC114.

Clusters are expected to have density profiles well approximated by the Navarro, Frenk, & White (1997) [NFW] profile,  $\rho \propto R^{-1}(R + R_s)^{-2}$ . However, in the radial range of interest here it is the inner profile, where the density distribution changes from  $\rho \sim R^{-1}$  to  $\rho \sim R^{-2}$ , that really matters. It has been argued (Williams, Navarro, & Bartelmann 1999) that a cluster with NFW profile cannot reproduce the angular distance of arcs from their cluster centers (for the dispersions of interest here,  $\sigma_{cl} \sim 800 - 1400$  km/s), and the steep inner profile of a BCG is needed. On the other hand, lensing studies of several clusters find that a core radius  $r_{core} \sim 30h^{-1}$  kpc is needed (e.g. Tyson, Kochanski, & Dell’Antonio 1998, Smail et al. 1996). Here we use isothermal spheres with  $r_{core} = 1$  or  $30h^{-1}$  kpc to bracket these results. A pure NFW profile would give results intermediate between these two cases.

There are several parameters that describe the galaxies. First, we use  $r_{core}^g = 0.1h^{-1}$  kpc throughout, in agreement with the constraints from quasar lensing studies (see e.g. Kochanek 1996). Second, we follow standard practice in lensing studies (see e.g. the discussion in Kochanek 1996) and assign a velocity dispersion to a galaxy using a Faber-Jackson (Faber & Jackson 1976) relation  $\sigma_g = \sigma_*(L/L_*)^{1/\beta}$ . The luminosity  $L$  is drawn from a Schechter distribution,  $(L/L_*)^\alpha \exp(-L/L_*)$  (Schechter 1976). The value of  $\beta$  ranges from  $\beta \sim 3$  in the B band to  $\beta \sim 4$  in the infrared (de Vaucouleurs & Olson 1982). Here we use  $\beta = 3$ ; our results do not change much if we use  $\beta = 4$  instead, as we discuss below.

Our next step is to choose the galaxy truncation radius,  $r_{cut}$ . The truncation of galaxy



halos inside clusters has been studied numerically by Klypin et al. (1999). An estimate of the size of a halo at distance  $R$  from a cluster center is given by the tidal radius  $r_t$ . For a galaxy and cluster with  $r_{core} = 0$ ,  $r_t = (\sigma_g/\sigma_{cl})R$ . Since we do not know the distance  $R$  for a galaxy at projected separation  $r$  from the cluster center, we use the average distance along the line of sight,  $\langle R \rangle = \int R(r, z) \rho(r, z) dz / \int \rho(r, z) dz$ . The galaxies that contribute the most to the arc cross section are those near the critical curve of the smooth cluster (see Fig. 1). Therefore, we evaluate  $\langle R \rangle$  at the Einstein radius,  $r \sim 60h^{-1}(\sigma_{cl}/1200 \text{ kms}^{-1})^2 \text{ kpc}$ . For  $\sigma_{cl} \sim 1200 \text{ km/s}$ , this is comparable to  $R_s$  for such a cluster (see Thomas et al. 1999). Thus, we evaluate  $\langle R \rangle$  at projected separation  $r = R_s$  and obtain  $\langle R \rangle \sim 2r$  for the NFW profile. Finally, we compare the rotation curve of a numerical halo (the typical example discussed by Klypin et al. 1999, bottom curve of their Fig. 6) to the model rotation curve of a truncated isothermal sphere, and obtain  $r_{cut} \sim 3r_t/4$ .

We shall take here  $\langle R \rangle = 100h^{-1} \text{ kpc}$ , and use throughout the paper  $r_{cut} = 3r_t/4$ . Therefore,  $r_{cut}^* = 15(\sigma_*/230 \text{ kms}^{-1})(\sigma_{cl}/1200 \text{ kms}^{-1}) h^{-1} \text{ kpc}$ . It is interesting to note that this value agrees fairly well with the value inferred from the effect of galaxies on the spatial distribution and orientation of the arcs and arclets in the cluster A2218 (see Kneib et al. 1996). The scaling of  $r_{cut}$  with  $\sigma_g$  implies that for a given cluster  $r_{cut} = r_{cut}^*(L/L_*)^\gamma$  with  $\gamma = 1/\beta = 1/3$ . Thus, the scalings of  $\sigma_g$  and  $r_{cut}$  with  $L$  are different from those suggested by Brainerd, Blandford, & Smail (1996) ( $\beta = 4$ ,  $\gamma = 1/2$ ), and used in the studies of A370, A2218 and AC114. However, we find the arc cross section to be very similar in either case because the galaxy mass-to-light ratio,  $M/L \propto \sigma_g^2 r_{cut}/L$ , is constant in both cases. Some authors have also explored  $\gamma = 0.8$  based on studies of the fundamental plane of ellipticals that suggest  $M/L \propto L^{0.3}$  (see Natarajan et al. 1998, and Bézecourt et al. 1999). It has been noted, however, that the fundamental plane can also be interpreted assuming constant  $M/L$  (Bender, Burstein, & Faber 1992), so the jury is still out on this question. Finally, we also note that we expect  $r_{cut}^* \propto \sigma_{cl}$  to be smaller for lower-dispersion clusters. This might

be part of the reason for the different  $r_{cut}^*$  obtained in the AC114 and A2218 analyses (see Natarajan et al. 1998 and Kneib et al. 1996, respectively).

In order to find the effect of galaxies on the arc cross section we must also choose their characteristic velocity dispersion  $\sigma_*$ , how they are distributed inside a cluster, and how many there are. Since galaxies too faint and/or too far from the critical curve do not contribute much to the arc cross section, we find it enough to include galaxies down to 2 mag fainter than  $L_*$  inside an area corresponding to  $150'' \times 150''$  for a cluster at redshift  $z_{cl} = 0.2$  (see Fig. 1). This will be our fiducial field of view (FOV) at this redshift, and we shall study a region of the same physical size at other redshifts. We are interested in clusters in the redshift range  $z_{cl} = 0.2 - 0.6$ , the range in which the arc cross section is large (see Bartelmann et al. 1998).

Smail et al. (1998) have studied a sample of 10 clusters at  $z_{cl} \sim 0.2$  with X-ray luminosities in the range of interest here. They find that the surface number density of red galaxies is  $\propto r^\delta$ , with  $\delta = -0.96 \pm 0.08$ , and that the luminosity distribution is well fit by a Schechter function with  $\alpha = -1.25$  and  $M_V^* = (-20.8 \pm 0.1) + 5\log h$ . Using  $M_V^* = -20.8$  and  $M_V = -20.35 - 8.5(\log\sigma_g - 2.3) + 5\log h$  (de Vaucouleurs & Olson 1982), we infer  $\sigma_* = 226$  km/s. From their Table 2 we infer a count of 20 – 40 galaxies (down to 2.3 mag fainter than  $L_*$ ) in a  $150'' \times 150''$  FOV, with a mean of 32. Furthermore, Smail et al. (1997) have studied a set of 10 clusters in the redshift range  $z_{cl} = 0.37 - 0.56$ . They find that elliptical galaxies are distributed with  $\delta = -0.8 \pm 0.1$  in the radial range of interest here, and their luminosities are well described by a Schechter function with  $\alpha = -1.25$ . Furthermore, we derive a count of 29 galaxies per cluster in a  $150'' \times 150''$  FOV for their clusters at  $z_{cl} \sim 0.4$  (down to 2 mag fainter than  $L_*$ ), consistent with a count of 20 at  $z_{cl} = 0.2$  assuming equal numbers in areas of equal physical size. We find that the same holds, within errors, for their clusters at  $z_{cl} \sim 0.54$ .

The previous results also agree with a homogeneous sample of clusters at low redshift (Lumsden et al. 1997). We infer a count of 17 galaxies in our FOV at  $z_{cl} = 0.2$  for the mean of the sample (down to 2 mag fainter than  $L_*$ , assuming  $\delta = -1$  and equal numbers in equal areas). However, most of these systems have low velocity dispersions. For the only cluster with  $\sigma_{cl} \sim 1200$  km/s, the fit parameters imply 30 galaxies. The mean  $M_{b_j}^* = -20.2$  implies  $\sigma_* = 232$  km/s, assuming a mean color  $b_j - V \sim .7$ . Finally, we also infer similar counts from the detailed study of 7 rich Abell clusters at  $z_{cl} \sim 0.15$  by Driver, Couch, & Phillipps (1998). They find  $\sim 50 - 150$  galaxies inside a  $280h^{-1}$  kpc radius (down to 3 mag fainter than  $L_*$ ; see their fig. 11). Thus, we infer  $19 - 57$  galaxies in our FOV, with a mean of 38 (down to 2 mag fainter than  $L_*$ , using their fig. 6 and assuming both  $\delta = -1$  and equal numbers in equal areas).

We shall summarize these observations by adopting  $\sigma_* = 230$  km/s and  $\alpha = -1.25$ . We shall assume a universal luminosity function, an adequate assumption for the inner region of rich clusters (see Driver, Couch, & Phillipps 1998). Finally, we shall take  $\delta = -1$ .<sup>2</sup> Therefore, the galaxies trace the dark matter, in agreement with gravitational lensing studies of clusters (see Tyson, Kochanski, & Dell’Antonio 1998; and references therein).

The choice of the number of galaxies in our FOV is complicated by the fact that it depends on the cluster velocity dispersion (Bahcall 1981). Girardi et al. (1999) have computed total cluster luminosities within fixed physical radii for a large, homogeneous sample of 89 clusters for which there is also velocity dispersion data. We have analyzed their data for luminosities inside  $0.5h^{-1}$  Mpc, and find that the data are well fit by a cluster luminosity  $L_{cl} \sim 6.3(\sigma_{cl}/770 \text{ kms}^{-1})^{1.5} \times 10^{11}h^{-2}L_{\odot}$ . There is, of course, significant scatter. This is believed to be physical, and results from the fundamental plane of clusters

---

<sup>2</sup> Strictly speaking, we distribute the galaxies in projection just like the cluster surface density profile, including flattening and core radius.

(Schaeffer et al. 1993) seen in projection. We find that 68% of the clusters have luminosities  $(.67 - 1.5)L_{cl}$ . Extrapolating the validity of  $L_{cl}$  to  $\sigma_{cl} = 1200$  km/s, we infer that there should be 37 galaxies in our fiducial FOV (assuming  $\delta = -1$  and equal numbers in equal areas). In view of this, and the previous discussion, we shall take  $N_g = 40$  galaxies inside a square  $316h^{-1}$  kpc on a side (our FOV at  $z_{cl} = 0.2$ ) for a cluster with  $\sigma_{cl} = 1200$  km/s, but we explore the range  $N_g = 20 - 60$  as representative of the likely scatter to be encountered. For clusters with different  $\sigma_{cl}$  we scale  $N_g$  by  $(\sigma_{cl}/1200 \text{ kms}^{-1})^{1.5}$ .

We finish this discussion of our choice of parameters by summarizing them in Table 1.

#### 4. Results

We have calculated  $\Delta$  for Monte Carlo realizations of the galaxy distribution in a cluster by ray tracing through a fine grid in the image plane (we find that  $0.375''$  spacing works well enough) to find the points that are imaged back to a given source. We take circular sources (this is adequate for our purpose of finding the cross section for very long arcs, for which the intrinsic ellipticity of the sources is not important) of  $1''$  diameter, and at redshift  $z_s = 1$ . Sources are placed with  $0.25''$  spacing or smaller depending on  $z_{cl}$ . Sets of contiguous pixels in the image plane that trace back to a given source are then an image. If at least one image has angular area at least 10 times the area of the source, the pixel area around the source position is added to the arc cross section.

Our main results are presented in Table 2, where we give the average  $\Delta$  of 10 realizations of the distribution of galaxies in a cluster,  $\langle\Delta\rangle$ . Results are given for a given cluster at three different redshifts and for three representative axial ratios  $q = q_3$  (i.e. the cluster is seen edge-on; see discussion below). The top row at each redshift gives results for a cluster with  $\sigma_{cl} = 1000$  km/s and  $r_{core} = 1(30)h^{-1}$  kpc, while the bottom row gives results

for  $\sigma_{cl} = 1200$  km/s and  $r_{core} = 1(30)h^{-1}$  kpc. The sources are assumed to be at redshift  $z_S = 1$ . Based on the scatter of 100 realizations of the galaxy distribution in a cluster at  $z_{cl} = 0.2$ , with  $q = 0.75$  and  $\sigma_{cl} = 1200$  km/s, we estimate the error for  $\langle\Delta\rangle$  in Table 2 to be  $\pm 0.02$ .

Thus, we see that typically  $\langle\Delta\rangle \lesssim 0.12$ . Increasing the number of galaxies to  $N_g = 60$  changes  $\langle\Delta\rangle$  only to  $\langle\Delta\rangle = 0.15$  from  $\langle\Delta\rangle = 0.11$  for our fiducial cluster at  $z_{cl} = 0.2$ :  $\sigma_{cl} = 1200$  km/s,  $r_{core} = 1h^{-1}$  kpc, and  $q = 0.75$ . Also, for the entire range  $\sigma_{cl} = 800 - 1400$  km/s we find that  $\langle\Delta\rangle = 0.07 - 0.15$  for the same cluster. The scatter introduced by the discrete nature of galaxies (the numerical scatter introduced by the finite size of our grids on the source and image planes is very small) is such that in 68% of the realizations  $\Delta$  is in the range  $\Delta = 0.03 - 0.16$ , again for our fiducial cluster. The results are not sensitive to the assumed source redshift. For  $z_S = 1.2$  or  $0.8$ ,  $\langle\Delta\rangle \sim .08$  for the same cluster. We do not find our neglect of the dependence of  $r_{cut}$  on the distance of a galaxy to the cluster center to be important either. We have used  $r_{cut} = (\sigma_g/\sigma_{cl})\langle R\rangle$ , where  $\langle R\rangle = (\pi/2)r$  for a galaxy at projected separation  $r$  if we assume  $\rho \propto R^{-3}$ , as appropriate for the more distant galaxies. We find that this changes  $\langle\Delta\rangle$  only to  $\langle\Delta\rangle = 0.13$  from  $\langle\Delta\rangle = 0.11$  for our fiducial cluster.

Our numbers are given for edge-on clusters for simplicity. However, the projection effect could significantly increase  $\langle\Delta\rangle$  only for fairly flattened clusters seen nearly face-on. For example, for a cluster at  $z_{cl} = 0.2$  with  $\sigma_{cl} = 1200$  km/s and  $r_{core} = 1h^{-1}$  kpc,  $\langle\Delta\rangle = 0.037$  if  $q_3 = q = 0.9$  (see Table 2). We find that this changes to  $\langle\Delta\rangle = 0.067$  instead if the cluster has  $q_3 = 0.5$ , and is seen in projection with  $q = 0.9$ . If we considered the cluster to be prolate instead,  $\langle\Delta\rangle$  would be smaller. Thus, our results for  $\langle\Delta\rangle$  are not significantly different when projection effects are taken into account.

We have assumed a Schechter luminosity function throughout. This often underestimates the number of bright galaxies in a cluster (see e.g. Lumsden et al. 1997).

We have corrected for this by assuming a luminosity function  $\propto (L/L_*)^\alpha \exp(-(L/L_*)^{1/4})$ . We find that this functional form (with the same  $\alpha$ ) fits the data better for  $L > L_*$ , without changing much the galaxy count for  $L < L_*$ . However, we find that with this luminosity function the value of  $\langle\Delta\rangle$  changes only to  $\langle\Delta\rangle = 0.12$  from  $\langle\Delta\rangle = 0.11$  for our fiducial cluster.

A possible concern is that these results apply only to a smooth cluster, whereas the clusters in the simulations are clearly substructured. However, we have done a realization of a substructured cluster by adding a large, secondary clump away from the center of the cluster, and described by a truncated isothermal sphere density profile with  $\sigma_{cl} = 500$  km/s and  $r_{core} = 1h^{-1}$  kpc. In this case we took  $r_{cut} = 225h^{-1}$  kpc  $\sim 2r$ , where  $r$  is the projected separation. This is clearly large given its velocity dispersion, but we took this value to maximize the effect of this subclump in the calculation. We find that even in this case, keeping the same total mass in our FOV as in the case of a smooth cluster with  $\sigma_{cl} = 1200$  km/s,  $\langle\Delta\rangle = 0.074$  instead of  $\langle\Delta\rangle = 0.11$ .

## 5. Discussion & Conclusions

Our main conclusion from this study is that the likelihood that a cluster generate long-arc images of background sources is not significantly enhanced by the presence of its galaxies. The many observationally based constraints that we have taken into account imply that there are simply not enough sufficiently massive galaxies in a cluster to affect significantly the probability of a long arc. The effect could be more significant for the probability of finding arcs of certain characteristics. For example, typically the long arcs appear isolated and aligned more or less perpendicular to the cluster major axis (Lupino et al. 1999). It can be seen in Figure 1 that the cross section for those arcs (the shaded area outside the left and right side of the tangential caustic in the top left panel) is enhanced

more by the presence of the galaxies:  $\Delta \sim 0.4$ . The effect would also be much larger for arclet statistics, which we have not addressed here.

Undoubtedly our treatment is simplified, but it is clear that the presence of galaxies within a cluster is a minor effect that cannot reconcile the observed frequency of arcs in clusters with the expectations in a universe dominated by a cosmological constant.

Meneghetti et al. (1999) have recently studied this problem with a different methodology. Our studies are fairly complementary. For example, their clusters have realistic large-scale substructure, whereas we explore more systematically the galaxy distribution parameter space. Our results are consistent; e.g. their ensemble of clusters with galaxies generate about 7% fewer long arcs than their pure dark matter clusters, a result entirely within the range we find here. Our results make it clear that the effect of galaxies is not necessarily to decrease the number of arcs, and that the number can be significantly larger in individual clusters.

Acknowledgments: One of us (RF) would like to acknowledge the organizers of the first Princeton-PUC Workshops on Astrophysics (held in Pucon, Chile, January 11-14, 1999) for their invitation to present our results prior to publication. AHM and JRP acknowledge support from NASA and NSF grants at UCSC.

## REFERENCES

- Bahcall, N. A. 1981, *ApJ*, 247, 787
- Bahcall, N. A., Ostriker, J. P., Perlmutter, S., & Steinhardt, P. J. 1999, *Science*, 284, 1481
- Bartelmann, M., Huss, A., Colberg, J. M., Jenkins, A., & Pearce, F. R. 1998, *A&A*, 330, 1
- Bender, R., Burstein, D., & Faber, S. M. 1992, *ApJ*, 399, 462
- Bézecourt, J., Kneib, J.-P., Soucail, G., Ebbels, T. M. D. 1999, *astro-ph/9810199*
- Binney, J. 1978, *MNRAS*, 183, 501
- Brainerd, T. G., Blandford, R. D., & Smail, I. 1996, *ApJ*, 466, 623
- Cooray, A. R. 1999, *A&A*, 341, 653
- de Vaucouleurs, G., & Olson, D. W. 1982, *ApJ*, 256, 346
- Driver, S. P., Couch, W. J., & Phillipps, S. 1998, *MNRAS*, 301, 369
- Faber, S. M., & Jackson, R. E. 1976, *ApJ*, 204, 668
- Girardi, M., Borgani, S., Giuricin, G., Mardirossian, F., & Mezzetti, M. 1999, *astro-ph/9907266*
- Grossman, S. A., & Narayan, R. 1988, *ApJ*, 324, L37
- Hamana, T., & Futamase, T. 1997, *MNRAS*, 286, L7
- Hattori, M., Watanabe, K., & Yamashita, K. 1997, *A&A*, 319, 764
- Kassiola, A., & Kovner, I. 1993, *ApJ*, 417, 450
- Keeton, C. R., & Kochanek, C. S. 1998, *ApJ*, 495, 157



- Klypin, A. A., Gottlober, S., Kravtsov, A. V., & Khokhlov, A. M. 1999 *ApJ*, 516, 530
- Kneib, J.-P., Ellis, R. S., Smail, I., Couch, W. J., & Sharples, R. M. 1996, *ApJ*, 471, 643
- Kochanek, C. S. 1996, *ApJ*, 466, 638
- Le Fèvre, O., Hammer, F., Angonin, M. C., Gioia, I. M., & Lupino, G. A. 1994, *ApJ*, 422, L5
- Lumsden, S. L., Collins, C. A., Nichol, R. C., Eke, V. R., & Guzzo, L. 1997, *MNRAS*, 290, 119
- Lupino, G. A., Gioia, I. M., Hammer, F., Le Fèvre, O., & Annis, J. A. 1999, *A&AS*, 136, 117
- Lynds, R., & Petrosian, V. 1986, *BAAS*, 18, 1014
- Meneghetti, M., Bolzonella, M., Bartelmann, M., Moscardini, L., & Tormen, G. 1999, *astro-ph/9907324*
- Natarajan, P., Kneib, J.-P., Smail, I., & Ellis, R. S. 1998, *ApJ*, 499, 600
- Navarro, J. F., Frenk, C. S., & White, S. D. M. 1997, *ApJ*, 490, 493
- Porter, A. C., Schneider, D. P., & Hoessel, J. G. 1991, *AJ*, 101, 1561
- Schechter, P. 1976, *ApJ*, 203, 297
- Schaeffer, R., Maurogordato, S., Cappi, A., & Bernardeau, F. 1993, *MNRAS*, 263, L21
- Smail, I., Dressler, A., Kneib, J.-P., Ellis, R. S., Couch, W. J., Sharples, R. M., & Oemler, A. 1996, *ApJ*, 469, 508
- Smail, I., Dressler, A., Couch, W. J., Ellis, R. S., Oemler, A., Butcher, H., & Sharples, R. M. 1997, *ApJS*, 110, 213

- Smail, I., Edge, A. C., Ellis, R. S., & Blandford, R. D. 1998, MNRAS, 293, 124
- Solinger, A. B., & Tucker, W. H. 1972, ApJ, 175, L107
- Soucail, G., Mellier, Y., Fort, B., & Picat, J. P. 1987, A&A, 172, L14
- Thomas, P. A. et al. 1999, MNRAS, 296, 1061
- Turner, E. L., Ostriker, J. P., & Gott, J. R. 1984, ApJ, 284, 1
- Tyson, J. A., Kochanski, G. P., & Dell’Antonio, I. P. 1998, ApJ, 498, L107
- Williams, L. L. R., Navarro, J. F., & Bartelmann, M. 1999, astro-ph/9905134
- Wu, X.-P., & Mao, S. 1996, ApJ, 463, 404
- Wu, X.-P., Xue, Y.-J., & Fang, L.-Z. 1999, astro-ph/9905106

Table 1. Model Parameters (Fiducial parameters marked with  $^\ddagger$ )

| Parameter | $\sigma_{cl}$          | $r_{core}$         | $q$                         | $\sigma_*$ | $r_{cut}^*$  | $r_{core}^g$ | $N_g$          | $\alpha$ | $\beta$ | $\gamma$ | $\delta$ |
|-----------|------------------------|--------------------|-----------------------------|------------|--------------|--------------|----------------|----------|---------|----------|----------|
|           | km/s                   | $h^{-1}$ kpc       |                             | km/s       | $h^{-1}$ kpc | $h^{-1}$ kpc |                |          |         |          |          |
| Value     | 1000, 1200 $^\ddagger$ | 1 $^\ddagger$ , 30 | 0.5, 0.75 $^\ddagger$ , 0.9 | 230        | 15           | 0.1          | 40 $^\ddagger$ | -1.25    | 3       | 1/3      | -1       |

Table 2. Average Galaxy Contribution to Arc Cross Section,  $\langle \Delta \rangle$

| redshift $z_{cl}$ | axial ratio $q$ |                |                |
|-------------------|-----------------|----------------|----------------|
|                   | 0.5             | 0.75           | 0.9            |
| 0.2               | 0.029(0.11)     | 0.060(0.009)   | -0.001(0.017)  |
|                   | 0.063(0.095)    | 0.11(0.12)     | 0.037(0.031)   |
| 0.4               | -0.052(-0.069)  | 0.047(0.025)   | 0.035(0.079)   |
|                   | 0.028(0.019)    | 0.11(0.071)    | 0.069(0.047)   |
| 0.6               | -0.095(-0.094)  | -0.042(-0.077) | -0.029(-0.061) |
|                   | -0.025(-0.04)   | 0.019(0.038)   | 0.039(0.061)   |

Fig. 1.— Results for our fiducial  $\sigma_{cl} = 1200$  km/s cluster. Top panels: source plane. Bottom panels: image plane. See text for further explanation.

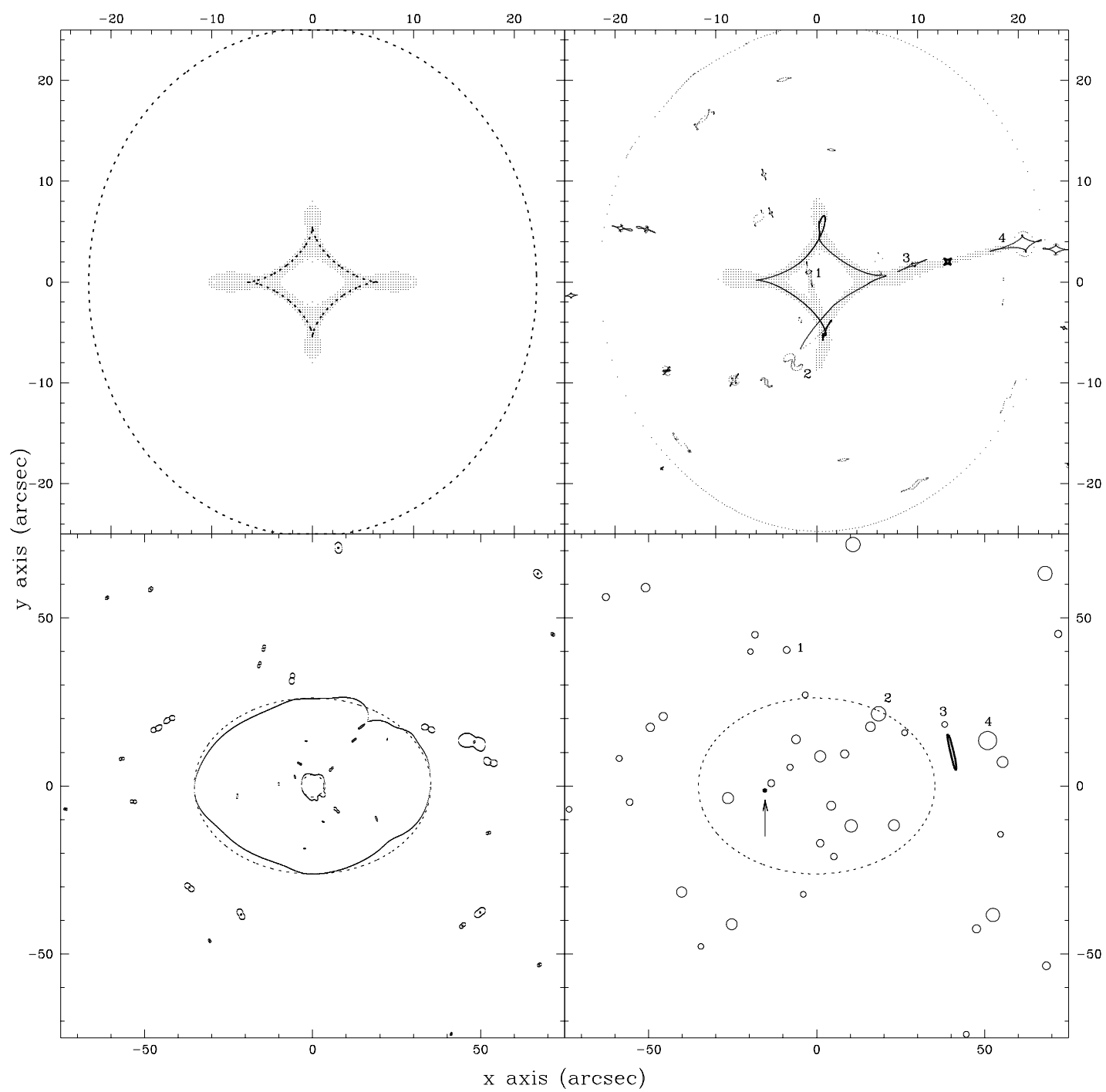


Figure 1